A Modular Soft Robotic Arm with Embedded Tactile Sensors for Proprioception

Wenye Ouyang*, Liang He, Alessandro Albini and Perla Maiolino

***Abstract*— Soft robotic arms are designed to execute dexterous tasks safely in cluttered environments due to their inherent compliance and infinite degrees of freedom. Closed-loop control requires proprioceptive sensing to retrieve the spatial configuration of the robot. However, the integration of soft sensing in the soft continuum body is still an ongoing challenge. In this paper, we present a highly integrated pneumatically actuated soft robotic arm that consists of 1) an omnidirectional actuator design for multi-material 3D printing, 2) a modular approach with fast assembling connectors and 3) a tactile sensing array embedded in the joint of each module. The in-joint placement of the tactile sensing array is used to map the variation of stress distribution between the two connected modules and the posture of the actuator with learned k-nearest neighbors regression. The experimental results showed that the method estimated the posture of a three-segment soft arm with a mean error of 5.64 mm for the tip location.**

I. Introduction

Soft robotics has become an emerging research area, opening up new possibilities and applications by creating resilient, adaptive, and safe robots which take advantage of their inherent compliance [1]. In particular, soft continuum robots have attracted the interest of many researchers because of their potential to be employed in a confined environment [2]. The objective is to increase the robot workspace with enhanced dexterity. The lengths of soft continuum robots determine their workspace, but solely increasing the length leads to difficulty in the control due to high redundancy and gravity effect in the system [3], and makes it hard to provide an accurate propriopceptive feedback.

Similar to rigid robotic arms, one solution is to adopt a modular design that allows to focus on the control and sensorisation of individual segments [4]. Relying on motion capture systems, several control methods have been proposed to realise feedback control of multisegment soft robotic arms [3], [5]. However, these solutions are unsuitable in environments where the visual feedback is impaired by obstacles and environmental lighting. Alternatively, a more robust solution is to introduce proprioception to the continuum robot to retrieve its spatial configuration. [6]. One method is to embed flexible and stretchable strain sensors such as piezoresistive and capacitive sensors in their soft bodies [7], [8]. These sensors deform with the soft bodies to measure directly the curvature of the robots. Using this method, [9]–[11] achieved the reconstruction of the complete spatial configuration of their soft continuum robots. However, the integration of these sensors is a non-trivial process that can change the mechanical properties of the soft body, affecting the robot motions. Another solution employs optical sensors to determine the bending direction and to measure the bending angle of an omnidirectional bending actuator [12] [13]. However, the integration of optical sensors becomes challenging when the number of modules composing the robot body increases. In [14] and [15], authors retrieved the bending angle of their bidirectional bending actuators using hall effect sensors. As the embedded magnets move relative to the sensors, the variations in the magnetic field are measured to estimate the curvature of the actuator. However, the rigidity of magnets hinders the integration and the performances are naturally influenced by the environmental magnetic field variations [6].

A different solution avoiding to embed sensors in the actuator's main body consist of placing a tactile sensor array on the top of each continuum segment. Our previous research [16] have shown that the postures of a tendon-driven soft robot can be retrieved using a tactile sensing array placed on the top. The preliminary study proves the method works on a single-segment continuum body. In this paper, we extend this in-joint sensorisation strategy to an integrated modular design of an omnidirectional bending pneumatic actuator. To capture critical bending motion of the actuator, 3D printed filtering pins are introduced to the actuator design to apply stress over the sensor. The pneumatic actuator is specifically designed with bellow structure and constraint beams to be suitable for multi-material 3D printing. The modular approach also included joint connectors to fast connect two

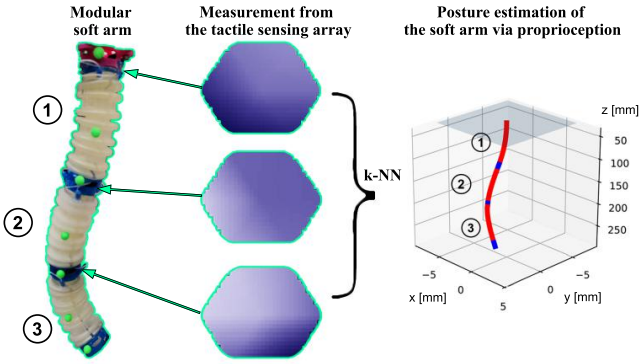

Fig. 1. The figure shows a three-segment soft arm with the proposed modular design. A hexagonal tactile array is embedded in the joint of each segment to measure the exerted stress distribution when the robot is moving. The figure shows the output of the three sensors as tactile images, where darker colours correspond to higher stress areas. In this study, the robot posture is reconstructed from the tactile measurements using a k-NN regressor.

The authors are with the Oxford Robotics Institute, University of Oxford, 23 Banbury Road, OX2 6NN, Oxford, UK

This work is supported by EPSRC Programme Grant 'From Sensing to Collaboration' (EP/V000748/1).

* Correspoding author email: wenye@robots.ox.ac.uk

segments together. As shown in Fig.1, the sensors are hosted inside the rigid part connecting two segments. Therefore, they could be easily integrated or removed after fabrication. It is worth noting that the integration of the tactile sensors does not change the mechanical properties of the soft robotic arm. Furthermore, since the sensors are embedded on the top of the segment, they do not directly interact with the environment. We performed experiments to characterize the design of the single module, showing the repeatability of bending motion and tactile sensor output. Then, considering a soft robot arm composed of three modules, we experimentally show that the tactile sensor output can be used to retrieve the shape of the robot body in a continuous form.

The rest of the paper is structured as follows. Section II describes the design and fabrication of the soft actuator. Section III explain the method used to exploit tactile measurements to retrieve the parameters describing the posture of a soft arm composed of three modules. The experimental methodology and results are presented in Sections IV and V respectively. Conclusion follows.

II. Design Of the Sensorised Soft Robotic Arm And Rationale

The modular soft robotic arm is designed for direct 3D printing, omnidirectional bending, and the integration of the in-joint tactile sensing arrays. The basic actuator design is adapted from [17], where the concept of internal beam constraints are used to control the bending motion.

A. Design Of the modular soft arm

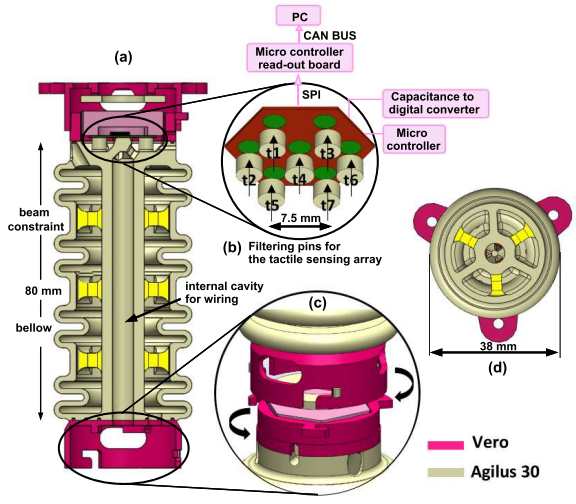

Fig. 2. Overview of soft robotic arm design (Colours indicate the material types and constraint beams are highlighted in bright yellow): **(a)** An axial view of the segment. The tactile sensing array is mounted on a hexagon holder and placed at the joint of the actuator. Three constraint sections can be seen in each chamber. **(b)** Detailed view of the contacts between CySkin and the cylinders on top of the segment. 7 soft cylinders are designed as morphological filters to amplify the tactile information, aligned with the 7 sensing taxels (t1-t7). **(c)** detailed view of the joint connection design showing how the relative position of two connected segments can be locked. Small cubes printed on the surface with Agilus 30 ensure a tight connection. **(d)** Radial view of the segment. Each chamber takes up 120 degrees.

Fig. 2 shows the overview of the modular soft arm design. The main body of the actuator consists of three enclosed chambers to achieve omnidirectional bending and a centre channel for passing through the pneumatic wires to connect to additional modules. The length and radius ratio of the actuator are based on our previous work in [17] and adapted to suit the size of the tactile sensing array. Bellow structure is introduced to achieve a larger bending angle with low driving pressure. Additional beam constraint is also introduced between two sections of the bellow structure to reduce axial expansion. The tactile sensing array is embedded within the 3D printed housing between the connecting joint of two modules. The sensor measures the variation of stress distribution from one bending segment to the attached segment. The housing of the tactile sensing array also functions as the connector to attach the two neighbouring segments. As can be seen in Fig. 2 (c), the connector can be easily locked or unlocked by rotating it clockwise or anticlockwise. Small soft cubes are printed on the surface of the bottom connector ring to ensure a tight connection.

B. In-joint tactile sensing array

The tactile array used in this work (namely *CySkin*) corresponds to an updated version of the tactile sensing technology presented in [18]. The CySkin module is composed of a flexible PCB containing 7 capacitive based transducers (namely *taxels*) evenly spaced of 7.5 mm, shown in Fig. 2(b). The CySkin module is covered with a conductive fabric acting as a ground plane. The change in the magnitude of stress over the sensor can cause a deformation of the dielectric layer. A 16-bit Capacitance to Digital Converter (CDC) and a microcontroller are embedded on the back of the PCB, capturing the variation of capacitance given by the deformation of the ground plane.

Considering the location and geometry of the 7 taxels on the hexagonal shaped CySkin sensor, 7 cylindrical features are designed to filter and augment the sensor readings to capture the stress distribution on the top while the robot is moving (schematics shown in Fig. 2(b)). As shown in Section IV, this information is used to create a model mapping the CySkin output with the robot configuration.

C. Fabrication of the modular soft arm

The modular soft arm is fabricated with a multi-material 3D printer (J735, Stratasys Ltd, USA), where multiple droplets of uncured material are deposited and blended and cured by UV light. The main body of the actuator is printed with Agilus30 (a soft and rubber-like material with a quoted tensile strength of 2.1-2.6MPa and a Shore hardness of 30A). The connector and the housing for the tactile sensing array are printed with Vero (a rigid plastic-like material with a quoted tensile strength of 50-65MPa and a Shore hardness of 83-86D). The monolithic fabrication solution allows the soft and rigid parts to be combined securely during the actuation. The soft arm is post-processed with chemical bathing to remove the internal support material in a tank (GEMINI SSR-550) filled with support removal solution (0.02 kg/L

Sodium Hydroxide and 0.01 kg/L Sodium Metasilicate).The net weight of the actuator is around 53g.

III. Soft Robotic Arm Shape Reconstruction from Tactile Measurements

This Section describes how tactile measurements can be used to estimate the shape of the soft robot. Different from [16], where the position of the tip was considered (for a single segment actuator), in this paper, we estimated the shape of the whole robot arm in a continuous form.

It is assumed to have a soft arm composed of three connected modules (described in Section II), each one hosting a tactile sensor array on the joint (rigid interconnection). The configuration of each soft segment is approximated using a Constant Curvature (CC) model. Therefore, the posture of the whole arm can be described using three parameters for each segment: the arc radius r, the arc angle θ and the angle ϕ of the plane where the arc is defined [19]. The soft robot posture can be then reconstructed by creating a model associating the tactile sensor responses with the posture of the robot described by r, θ, ϕ.

A. Soft Robotic Arm Kinematic Description

Three segments are interconnected by rigid connectors forming a kinematic chain as shown in Fig. 3. The spatial configuration the i-th module is approximated with a CC model and thus defined by three kinematic parameters r_i, θ_i and ϕ_i [19], as shown in Fig. 3(b). Fig. 3(a) illustrates the kinematic model of the three-segment soft robotic arm, considering the rigid interconnection, where $\{S_0\}$ is the base frame and $\{S_i\}$ defines the frame at the end of rigid connector fixed to the tip of the $i-$th arc. The position and orientation of the tip of the $i-$th segment with respect to its parent frame $\{S_{i-1}\}$ can be expressed with the following transformation matrix:

$$T^i_{i-1}(r_i,\theta_i,\phi_i) = \bar{T}^i_{i-1}(r_i,\theta_i,\phi_i)\begin{bmatrix} I_3 & \mathbf{d} \\ \mathbf{0} & 1 \end{bmatrix} \quad (1)$$

where I_3 is the 3×3 identity matrix and $\mathbf{d} = [0,0,d]^\intercal$, with $d \in \Re$ representing the constant length of the rigid connection. The transformation matrix $\bar{T}^i_{i-1}(r_i,\theta_i,\phi_i)$ based on the CC approximation has the following structure:

$$\bar{T}^i_{i-1}(r_i,\theta_i,\phi_i) = \begin{bmatrix} R^i_{i-1}(\theta_i,\phi_i) & \mathbf{p}^i_{i-1}(r_i,\theta_i,\phi_i) \\ \mathbf{0} & 1 \end{bmatrix} \quad (2)$$

where $R^i_{i-1}(\theta_i,\phi_i) \in \Re^{3\times3}$ and $\mathbf{p}^i_{i-1}(r_i,\theta_i,\phi_i) \in \Re^{3\times1}$ correspond to the rotation matrix and the translation vector defined in [19].

B. k-NN Regression for Shape Reconstruction

According to Section III-A, the configuration of the whole robot can be described by the following vector of parameters:

$$\boldsymbol{\beta} = [r_1,\theta_1,\phi_1,r_2,\theta_2,\phi_2,r_3,\theta_3,\phi_3]^\intercal \quad (3)$$

It is also assumed that at a given time instant the tactile sensors provide a set of measurements $\mathrm{P} = \{p_1,p_2,\ldots,p_N\}$ where N is the number of taxels. As previously described,

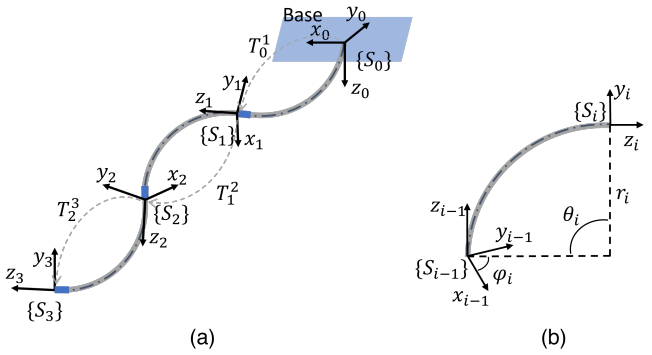

Fig. 3. (a) The kinematic model of the three segment soft robotic arm. (b) The kinematic parameters of i-th segment

the goal is to define a model $M(\mathrm{P}) \rightarrow \boldsymbol{\beta}$ mapping the raw taxel responses obtained for a given robot configuration with the parameters describing it. Due to the complexity of modelling the relationship between the arm configuration and the stress distribution sensed by the tactile arrays, we considered a data-driven approach to learn this mapping. Among the possible machine learning based models, in this paper, the use of a k-NN regressor has been considered for this task. The rationale behind this choice is given in [20], where the current applications of machine learning in the field of soft robotics are reviewed. They compared several machine learning techniques employed as regression models to predict the deformations of soft robots, concluding that k-NN provides the best overall performance with low average error and model bias.

The dataset used to train the k-NN model consists of H pairs of samples P_h and $\boldsymbol{\beta}_h$ corresponding to the tactile readings and the configuration parameters related to a specific robot posture respectively. The output of the k-NN regressor corresponds to $\hat{\boldsymbol{\beta}}_h$, i.e. the estimated kinematic parameters, defined as follows:

$$\hat{\boldsymbol{\beta}} = [\hat{r}_1,\hat{\theta}_1,\hat{\phi}_1,\hat{r}_2,\hat{\theta}_2,\hat{\phi}_2,\hat{r}_3,\hat{\theta}_3,\hat{\phi}_3]^\intercal \quad (4)$$

Further details on the size of the dataset H and on the data collection and training procedure are given in Section IV-C.

IV. Methodology

A. Experimental Setup

To operate the multisegment soft robotic arm, a pneumatic actuation system was built to control the multiple chambers independently. Since the soft arm is composed of three soft modules, each one having three chambers, the control system needs to control the actuation pressure of 9 chambers. As showed in Fig. 4(b), representing the control system of a single segment, three 60 mL syringes were connected to the three chambers through silicone pipes. The plunger flanges of the syringes are driven by three stepper motors which allow precise control of the pressures inside the corresponding chambers. A pressure sensor (ADP51A11, Panasonic, Japan) was used to measure the pressures inside the chambers. All components used for actuating one module were connected to

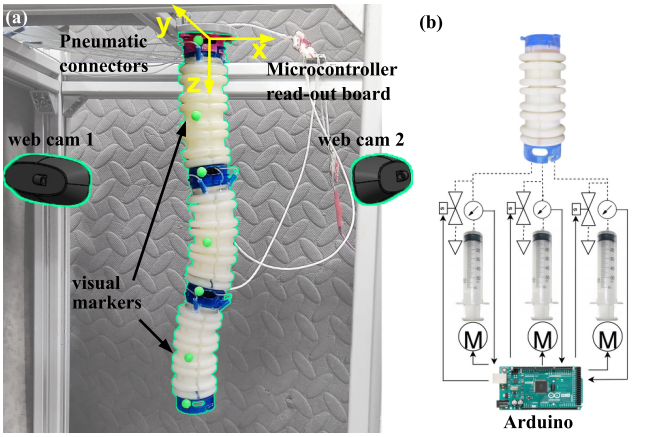

Fig. 4. **(a)** Front view of the experimental setup. Two cameras are used to retrieve the 3D positions of the green visual markers placed on the robot arm; **(b)** Schematics of the pneumatic actuation system for a single soft segment. Three identical systems are used to control the three-segment design.

an Arduino Mega 2560 board, implementing a PI controller that regulates the pressure inside the chambers by controlling the movements of the motors. The desired actuation pressure is commanded from an external computer to the Arduino through serial communication.

As visible in Fig. 4(a), green visual markers are attached to the robot body. The 3D coordinates of the markers (attached to the top, middle and bottom of each segment) were captured using two Logitech C270 cameras. The position of the marker is then used to retrieve the ground-truth spatial configuration of the robot and compute the kinematic parameters needed to train and evaluate the k-NN regressor. The system collects 21 tactile measurements (7 for each segment) at 20 Hz.

B. Soft Segment Characterisation

This section describes the experiments performed to characterise the proposed design. In particular, we focused on characterising: (i) the motion of the actuator, testing both the repeatability of the bending angle and tactile measurements corresponding to a given input pressure; (ii) the CySkin output when the tip of the soft module is moved to a specific position by commanding pressures to the chambers and when subjected to external forces.

The first experiment was conducted by actuating the soft module such that the plane angle ϕ was constant during the whole characterisation. A single chamber was actuated with a pressure ranging in $[0, 15]$ KPa with increments of 0.5KPa. The bending angle and the current actuation pressure were recorded at the steady-state. At the end of the procedure, the actuator was fully deflated. This experiment was performed 5 times to test both the repeatability of the motion and tactile measurements. The same experiment was executed by inflating two chambers simultaneously with the same amount of pressure.

The second characterization experiment is aimed at evaluating how the stress distribution on the top of the module changes when the robot is pneumatically actuated or subjected to an external force. The tip of the segment, corresponding to the 3D position of the green marker attached to the rigid section (see Fig. 4(a)), was moved in a workspace of radius 25 mm in two different ways: (i) using the control system to command 470 random pressure values in the interval [0,15] KPa; (ii) by placing an obstacle in contact with the tip of the segment in 470 arbitrary locations (see Fig. 5). The CySkin response was collected when the actuator was in a steady-state condition.

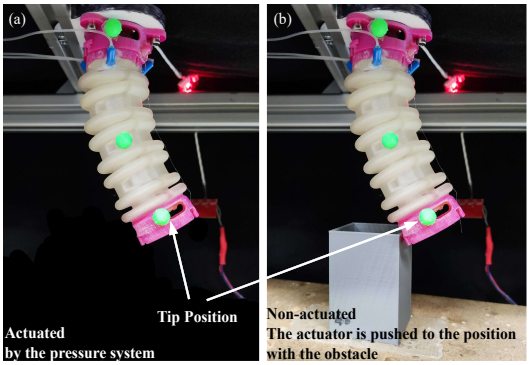

Fig. 5. The experimental setup for characterising how the stress distribution on the top of the module changes in regard to the tip position. A comparison study is done between the pneumatic actuated case and external contact case. **(a)** The actuator is actuated by the pressure system to allow the tip to be freely explored in the workspace (a circle with a diameter of 25 mm in the XY-plane). **(b)** The actuator is pushed to the configuration to allow the tip position maintained in the same workspace. The actuator is not actuated by the internal pressure.

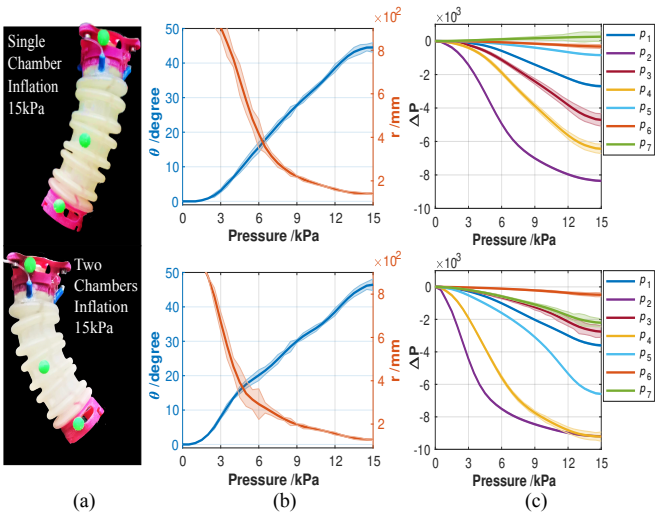

Fig. 6. Module bending characterisation. **(a)** The bending motion of the module when one chamber is inflated (top) and two chambers are inflated to the same amount of pressure (bottom); **(b)** and **(c)** illustrate the actuation pressure against the bending angle θ and taxel responses, respectively when one (top) or two chambers (bottom) are inflated.

C. Data Collection and Model Training

To train and evaluate the k-NN classifier we collected a dataset of pairs $\{\mathrm{P}_h, \boldsymbol{\beta}_h\}$ corresponding to the 21 tactile readings and the 9 kinematic parameters associated to the h-th robot posture.

The soft arm was actuated to generated $H = 908$ unique spatial configurations. The robot postures were generated, by commanding a set of desired pressures to the 9 chambers

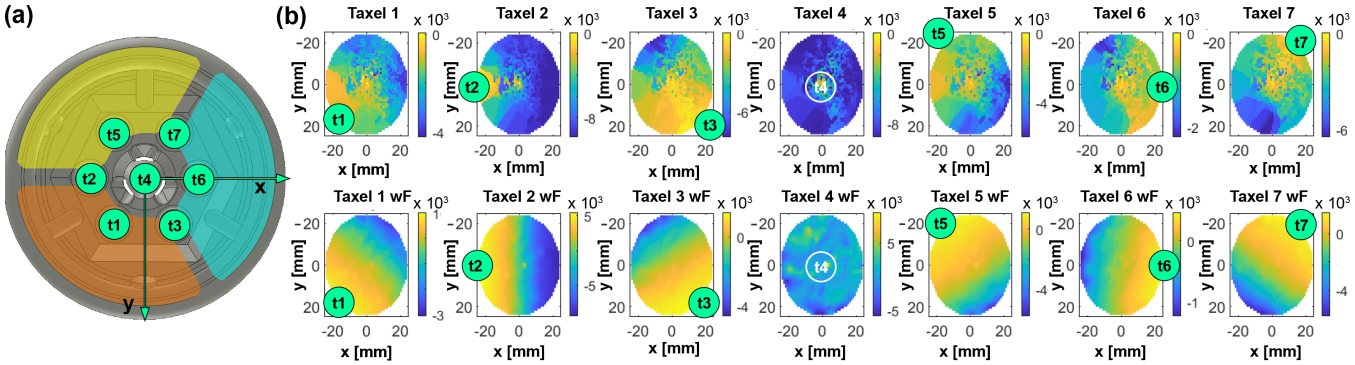

Fig. 7. CySkin sensor output in two different scenarios. Setup see Fig. 5. **(a)** A top view of the chambers of the module with the highlighted positions of the taxels (t1-t7). **(b)** The colourmap of each subfigure represents the steady-state response of the single taxel when the actuator tip is actuated at the specific x and y location in the workspace. The marker indicates the direction of the taxel in regard to the workspace origin. The characterised Cartesian workspace of the actuator is illustrated as a circle with a radius of 25 mm. The top row figures show the response of each taxel when the soft module is actuated, while the bottom row shows the response when the actuator is subjected to an external force. The colourmap was generated from the 470 samples by resampling the workspace using a regular grid and interpolating the output of the sensors using a Nearest Neighbor approximation.

randomly picked from an interval ranging from [0,15] KPa with increments of 0.5 KPa.

When the robot reached the steady-state, the tactile data sample P_h was collected. Furthermore, the parameters $\boldsymbol{\beta}_h$ describing the configuration of each segment under CC assumption, were computed from the position of green markers placed along the soft robot arm as described in [21].

The dataset was split in train (80%) and test (20%) sets. The model was trained using the cosine similarity [22] between $\hat{\boldsymbol{\beta}}$ and $\boldsymbol{\beta}$ as distance metric (angles have been converted into unitary vectors when computing the distance). Furthermore, since the k-NN regressor requires a proper choice of the parameter k avoiding to overfit or underfit the data, a 3-fold cross-validation [23] has been performed on the training data, leading to the choice of $k = 4$.

V. Results

A. Soft Robot Characterisation

Fig. 6 summarise the results of the 5 experiments performed to characterize the motion of the soft module and its repeatability. In particular, Fig. 6(a) shows the photographs of the module and indicates the chambers actuated during the experiment, Fig. 6(b) shows the relations pressure/angle, reporting both the average and standard deviation among the 5 experiments. Similarly, Fig. 6(c) reports the average and standard deviation of the tactile sensing response at a given pressure. It can be seen from Fig. 6(b) and 6(c) that proposed design present good repetability both in terms of bending angle and tactile measurements obtained for the given input pressure, presenting a low standard deviation across the five trials.

Fig. 7 shows the result of the second characterization experiment. The spatial distribution of the tactile sensing array is showed in Fig. 7(a), while Fig. 7(b) contains a number of subplot each one showing a top view of the workspace reached by the tip of the segment. The color associated to a position in the space, is related to the response of the specific taxel when the module is actuated with the control system (first row) and when subjected to an external force (second row). The figure shows that the taxels outputs (except t_4) are strongly correlated to the tip location. The 4-th taxel only exhibits a clear response when the actuator is at the origin. It can be also seen that taxels t_1, t_3, t_5 and t_6 shows a similar pattern in the responses when subjected to external forces compared to the responses obtained actuating the module in the free space. However, the magnitude of the response is different. Although beyond the scope of this paper, this opens to a possible future extension of the work, where the tactile measurement can be used to provide exteroceptive sensing by detecting the presence of contacts on the robot arm.

TABLE I

Mean Estimation Error for Each Parameter Describing the Robot Posture

	$\bar{e}_r$ (mm)	$\bar{e}_\theta$ (rad)	$\bar{e}_\phi$ (rad)
Module 1	53.86	0.028	0.096
Module 2	38.90	0.033	0.069
Module 3	45.95	0.038	0.051

B. Proprioception of Soft Robotic Arm

To evaluate the performance of the k-NN regression, we computed the error between the parameters $\boldsymbol{\beta}$ (collected with the cameras) and the estimated parameters $\hat{\boldsymbol{\beta}}$. Table I shows the result of the k-NN regressor applied on the test data, reporting for each one of the three modules, the mean estimation errors $\bar{e}_r$, $\bar{e}_\theta$ and $\bar{e}_\phi$ for the tree kinematic parameters.

As it can be seen from Fig. 8, the low estimation error allow to correctly reconstruct the current posture of the robot body. Furthermore, $\hat{\boldsymbol{\beta}}$ can be substituted on the equation describing the forward kinematic (see Section III-A) to obtain the position of the tip of the soft arm. The parameters $\hat{\boldsymbol{\beta}}$ related to the results presented in Table I, allow to estimate the position of the tip with a mean error $\bar{e}_x = 5.64$ mm and with a low standard deviation $\sigma_x = 1.91$ mm. The error is computed on the test set as the Euclidean distance between the predicted and the real tip position captured using the two cameras.

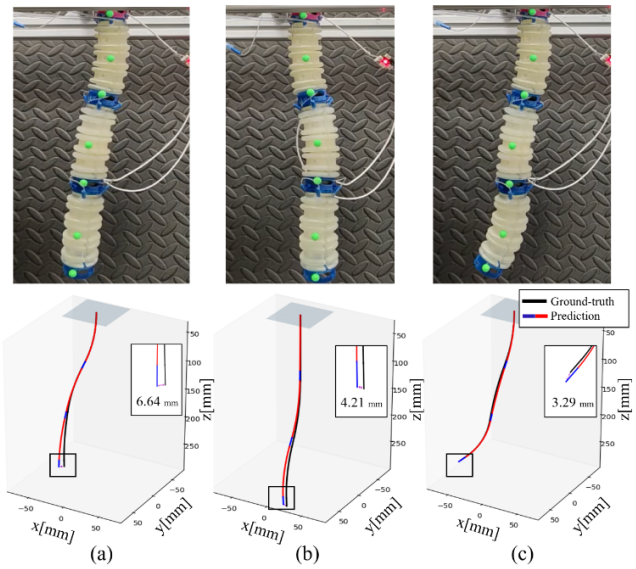

Fig. 8. Examples of the posture reconstruction obtained using the k-NN regressor. The top row show pictures of the soft arm and the bottom row show the corresponding plots of the ground-truth and predicted configurations. In the plots, the black and red-blue lines represent the real and estimated posture of the robot. Close views of the tip positions are provided with a double direction arrow indicating the prediction error. The corresponding kinematic parameters $\boldsymbol{\beta}$ and $\hat{\boldsymbol{\beta}}$ are: (a) [248.29, 0.380, 1.830, 458.12, 0.203, 4.485, 601.57, 0.151, 5.026] and [269.15, 0.343, 1.894, 398.47, 0.226, 4.557, 697.14, 0.125, 5.073], (b) [507.65, 0.189, 0.786, 254.16, 0.354, 3.156, 289.51, 0.311, 5.589] and [416.19, 0.211, 0.736, 265.31, 0.368, 3.097, 261.76, 0.344, 5.514], (c) [345.65, 0.276, 1.729, 498.68, 0.187, 4.626, 145.73, 0.621, 2.351] and [397.49, 0.239, 1.816, 443.98, 0.212, 4.673, 151.25, 0.603, 2.384].

VI. Conclusion

In this paper, a modular soft robotic arm providing omnidirectional bending and designed for direct 3D printing was presented. Tactile sensor arrays are placed at the joint of the modular segments to measure the stress distribution while the robot is moving. Compared to embedding sensors along the deformed soft body of the actuator, the integration of the tactile sensors at the joint does not change the mechanical properties of the actuator and does not interfere with the robot motion. The sensors also experience less relative movement and fatigue, with a potential of an increased lifetime. Moreover, we experimentally showed that the relation between the tactile sensor responses and the spatial configuration of the robot can be learnt by performing a k-NN regression. According to what was discussed in Section V-A, the stress distribution pattern generated by an external force is different to the one generated through pneumatic actuation. This open to a possible extension of this work, where tactile measurements can be exploited to detect the presence of external forces acting on the robot body.

References

[1] D. Rus and M. T. Tolley, "Design, fabrication and control of soft robots," *Nature*, vol. 521, no. 7553, pp. 467–475, 2015.

[2] S. Satheeshbabu, N. K. Uppalapati, T. Fu, and G. Krishnan, "Continuous control of a soft continuum arm using deep reinforcement learning," in *2020 3rd IEEE International Conference on Soft Robotics (RoboSoft)*. IEEE, 2020, pp. 497–503.

[3] R. K. Katzschmann, M. Thieffry, O. Goury, A. Kruszewski, T.-M. Guerra, C. Duriez, and D. Rus, "Dynamically closed-loop controlled soft robotic arm using a reduced order finite element model with state observer," in *2019 2nd IEEE International Conference on Soft Robotics (RoboSoft)*. IEEE, 2019, pp. 717–724.

[4] B. T. Phillips, K. P. Becker, S. Kurumaya, K. C. Galloway, G. Whittredge, D. M. Vogt, C. B. Teeple, M. H. Rosen, V. A. Pieribone, D. F. Gruber *et al.*, "A dexterous, glove-based teleoperable low-power soft robotic arm for delicate deep-sea biological exploration," *Scientific reports*, vol. 8, no. 1, pp. 1–9, 2018.

[5] C. Della Santina, R. K. Katzschmann, A. Bicchi, and D. Rus, "Model-based dynamic feedback control of a planar soft robot: trajectory tracking and interaction with the environment," *The International Journal of Robotics Research*, vol. 39, no. 4, pp. 490–513, 2020.

[6] H. Wang, M. Totaro, and L. Beccai, "Toward perceptive soft robots: Progress and challenges," *Advanced Science*, vol. 5, no. 9, p. 1800541, 2018.

[7] C. Lucarotti, M. Totaro, A. Sadeghi, B. Mazzolai, and L. Beccai, "Revealing bending and force in a soft body through a plant root inspired approach," *Scientific reports*, vol. 5, no. 1, pp. 1–10, 2015.

[8] Z. Xie, F. Yuan, Z. Liu, Z. Sun, E. M. Knubben, and L. Wen, "A proprioceptive soft tentacle gripper based on crosswise stretchable sensors," *IEEE/ASME Transactions on Mechatronics*, vol. 25, no. 4, pp. 1841–1850, 2020.

[9] G. Soter, A. Conn, H. Hauser, and J. Rossiter, "Bodily aware soft robots: integration of proprioceptive and exteroceptive sensors," in *2018 IEEE international conference on robotics and automation (ICRA)*. IEEE, 2018, pp. 2448–2453.

[10] Y. Toshimitsu, K. W. Wong, T. Buchner, and R. Katzschmann, "Sopra: Fabrication & dynamical modeling of a scalable soft continuum robotic arm with integrated proprioceptive sensing," *arXiv preprint arXiv:2103.10726*, 2021.

[11] R. L. Truby, C. Della Santina, and D. Rus, "Distributed proprioception of 3d configuration in soft, sensorized robots via deep learning," *IEEE Robotics and Automation Letters*, vol. 5, no. 2, pp. 3299–3306, 2020.

[12] S. Sareh, Y. Noh, M. Li, T. Ranzani, H. Liu, and K. Althoefer, "Macrobend optical sensing for pose measurement in soft robot arms," *Smart Materials and Structures*, vol. 24, no. 12, p. 125024, 2015.

[13] I. Van Meerbeek, C. De Sa, and R. Shepherd, "Soft optoelectronic sensory foams with proprioception," *Science Robotics*, vol. 3, no. 24, 2018.

[14] M. Luo, E. H. Skorina, W. Tao, F. Chen, S. Ozel, Y. Sun, and C. D. Onal, "Toward modular soft robotics: Proprioceptive curvature sensing and sliding-mode control of soft bidirectional bending modules," *Soft robotics*, vol. 4, no. 2, pp. 117–125, 2017.

[15] S. Ozel, N. A. Keskin, D. Khea, and C. D. Onal, "A precise embedded curvature sensor module for soft-bodied robots," *Sensors and Actuators A: Physical*, vol. 236, pp. 349–356, 2015.

[16] L. Scimeca, J. Hughes, P. Maiolino, and F. Iida, "Model-free soft-structure reconstruction for proprioception using tactile arrays," *IEEE Robotics and Automation Letters*, vol. 4, no. 3, pp. 2479–2484, 2019.

[17] L. He, X. Tan, K. Suzumori, and T. Nanayakkara, "A method to 3d print a programmable continuum actuator with single material using internal constraint," *Sensors and Actuators A: Physical*, vol. 324, p. 112674, 2021.

[18] A. Schmitz, P. Maiolino, M. Maggiali, L. Natale, G. Cannata, and G. Metta, "Methods and technologies for the implementation of large-scale robot tactile sensors," *IEEE Transactions on Robotics*, vol. 27, no. 3, pp. 389–400, 2011.

[19] R. J. Webster III and B. A. Jones, "Design and kinematic modeling of constant curvature continuum robots: A review," *The International Journal of Robotics Research*, vol. 29, no. 13, pp. 1661–1683, 2010.

[20] D. Kim, S.-H. Kim, T. Kim, B. B. Kang, M. Lee, W. Park, S. Ku, D. Kim, J. Kwon, H. Lee *et al.*, "Review of machine learning methods in soft robotics," *Plos one*, vol. 16, no. 2, p. e0246102, 2021.

[21] Z. Gong, J. Cheng, K. Hu, T. Wang, and L. Wen, "An inverse kinematics method of a soft robotic arm with three-dimensional locomotion for underwater manipulation," in *2018 IEEE International Conference on Soft Robotics (RoboSoft)*. IEEE, 2018, pp. 516–521.

[22] P.-N. Tan, M. Steinbach, and V. Kumar, *Introduction to Data Mining*. Addison Wesley, May 2005.

[23] R. Kohavi *et al.*, "A study of cross-validation and bootstrap for accuracy estimation and model selection," in *Ijcai*, vol. 14, no. 2. Montreal, Canada, 1995, pp. 1137–1145.